







Eastern Mediterranean water outflow during the Younger Dryas was twice that of the present day

Sergio Trias-Navarro ^{1,2✉}, Leopoldo David Pena¹, Maria de la Fuente ¹, Eduardo Paredes ¹, Ester Garcia-Solsona¹, Jaime Frigola ¹, Albert Català¹, Antonio Caruso², Fabrizio Lirer³, Negar Haghipour⁴, José Noel Pérez-Asensio ⁵ & Isabel Cacho ¹

Eastern Mediterranean deep-intermediate convection was highly sensitive to varying inputs of fresh water fluxes associated with increased rainfall during the African Humid period (15–6 kyr Before Present). Here we investigate changes in the water-outflow from the Eastern Mediterranean Sea since the last deglaciation using neodymium isotope ratios. Our results indicate enhanced outflow during the Younger Dryas, two times higher than present-day outflow and about three times higher than during the last Sapropel. We propose that the increased outflow into the western Mediterranean over the Younger Dryas was the result of the combined effect of 1) enhanced climate-driven convection in the Aegean Sea and 2) reduced convection of western deep water during this period. Our results provide solid evidence for an enhanced Younger Dryas westward flow of Eastern Mediterranean sourced waters in consonance with an intensification of Mediterranean water-outflow during a weakened state of the Atlantic circulation.

¹GRC Geociències Marines, Departament de Dinàmica de la Terra i de l'Oceà, Facultat de Ciències de la Terra, Universitat de Barcelona, Campus de Pedralbes, C/Martí i Franquès s/n, 08028 Barcelona, Spain. ²Dipartimento di Scienze Biologiche Chimiche e Farmaceutiche, Via Archirafi 18, 90123 Palermo, Italy. ³Dipartimento di Scienze della Terra, Sapienza Università di Roma, P. Aldo Moro 5, 00185 Roma, Italy. ⁴Department of Earth Sciences, ETH Zurich, Sonneggstrasse 5, 8092 Zurich, Switzerland. ⁵Departamento de Estratigrafía y Paleontología, Facultad de Ciencias, Universidad de Granada, Campus de Fuentenueva s/n, Granada 18002, Spain. ✉email: sergildt@gmail.com

The Mediterranean Sea hydrography is typically characterized by a negative net precipitation-evaporation balance across the basin. As a result of this deficit, the Mediterranean Sea thermohaline circulation system (Med-THC) presents an anti-estuarine pattern, where the inflowing fresh and cold Atlantic surface waters entering through the Strait of Gibraltar, progressively transform into saltier surface waters, that eventually sink to intermediate depths at the Levantine Sea as Levantine Intermediate Water (LIW). The LIW contributes to pre-conditioning deep water convection both in the Adriatic Sea and the Aegean Sea, where the Eastern Mediterranean Deep Water (EMDW) is formed. EMDW and LIW outflow together through the Strait of Sicily, hereafter called Eastern Mediterranean Source Waters (EMSW), contributing also to the convection of deep waters at the Gulf of Lions to produce Western Mediterranean Deep Water (WMDW). Both WMDW and EMSW eventually outflow into the Atlantic Ocean through the Strait of Gibraltar forming the so-called Mediterranean Outflow Water (MOW), thus closing the Med-THC system (Fig. 1a)^{1–4}.

Accordingly, the Mediterranean Sea and the Atlantic Ocean behave as a closely coupled system connected through the Strait of Gibraltar and therefore, changes in the Atlantic hydrography could induce changes in the Med-THC and vice versa. In this regard, some studies have hypothesized on the potential role that past climate changes might have exerted in modifying MOW physico-chemical properties, that by extension could have induced changes in the Atlantic Meridional Overturning Circulation^{5–7}. Several proxies show evidence that the intensity of

the Med-THC system is highly sensitive to past climate oscillations at different timescales and in some particular periods^{8–11}. In particular, last deglacial sea level rise and the associated increase of Atlantic fresh-water inflow through the Strait of Gibraltar promoted surface water stratification, that caused a generalized weakening of deep water convection at Gulf of Lions^{11,12}. Increased water column stratification also promoted poorly-oxygenated conditions at depth that consequently led into the formation of the last Organic Rich layer at the deep western Mediterranean basin (15–8.9 kyr Before Present or hereafter BP, 1950 as the commencement date of the age scale) (Cacho et al. 2002; Pérez-Asensio et al. 2020; Rogerson et al. 2008).

The development of the last Organic Rich layer coincided with the onset of the so-called African Humid Period (from ~15 to 6 kyr BP) driven by the intensification of the African Monsoon that led to increased runoff from north African riverine systems into the Eastern Mediterranean (E-Med) basin^{13–16}. It has been argued that generalized freshening of surface waters through runoff promoted a stronger sea surface density stratification that consequently weakened intermediate and deep water convection of the E-Med prior to the Sapropel formation, although such pre-conditioning phase has been largely debated^{18,17,18}. Interestingly, the Atlantic Meridional Overturning Circulation slowdown associated with the Younger Dryas (YD; from 12.95 to 11.65 kyr BP) involved worldwide changes in precipitation patterns^{19–21}. In particular, a weakening of the monsoon precipitation in North Africa caused an important decrease of freshwater supply toward the Mediterranean Sea^{14,17,22,23}, while overall cold and arid

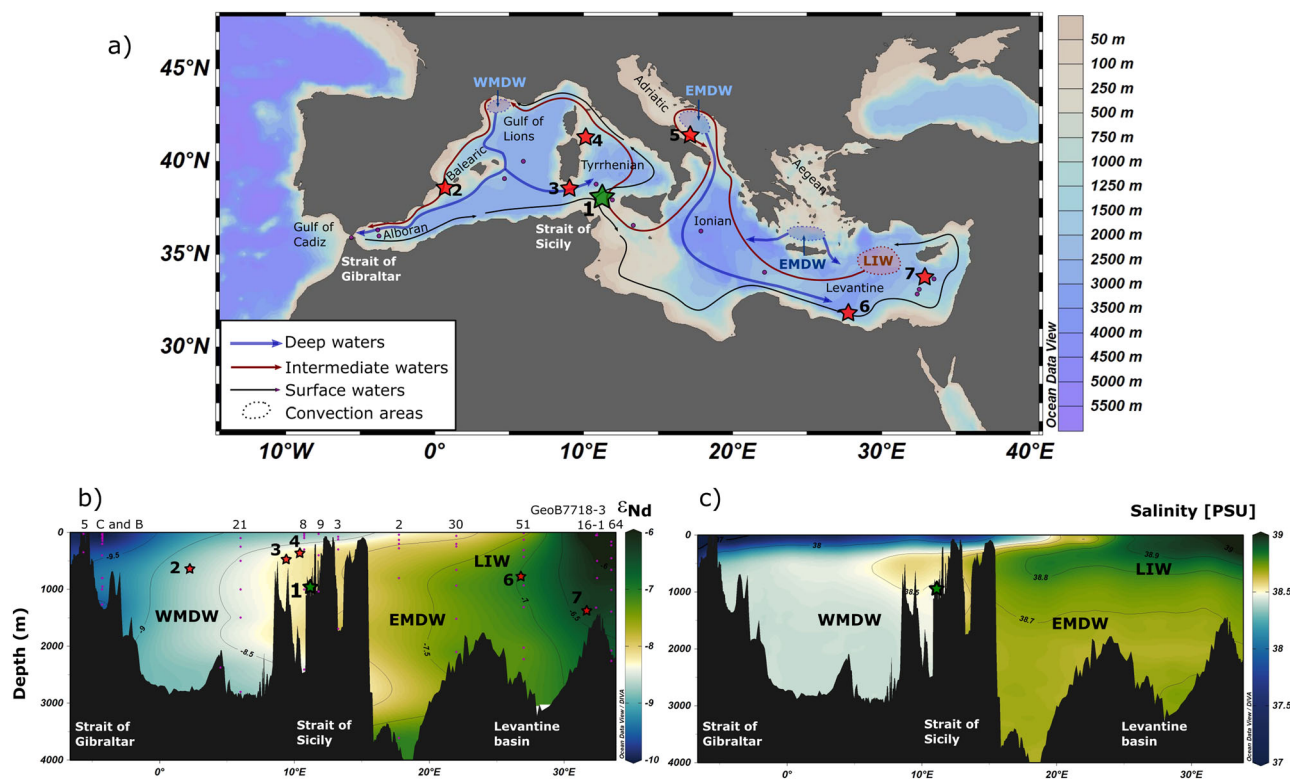


Fig. 1 Neodymium and salinity modern values of the Mediterranean Sea. **a** Map of the study area in the Mediterranean Sea. Modern surface and deep hydrology of western and eastern Mediterranean Sea represented in the map is based on ref. 2–4. Basic map of the Mediterranean Sea obtained from Ocean Data View. The green star represents the studied core NDT-6-2016 (1) and red stars represent the other cores discussed in this manuscript located in both the western and eastern Mediterranean Sea: 2) SU92-33 and 3) RECORD23⁴¹, 4) MD01-2472 and 5) MD90-917³⁹, 6) MS27PT⁴² and 7) BC07⁵¹. Violet circles stand for the stations of the obtained present-day seawater ϵ_{Nd} values. Blue arrows indicate deep waters (Western -WMDW- and Eastern -EMDW- Mediterranean Deep Waters), red arrows represent Levantine Intermediate Water (LIW) and black ones the surface Modified Atlantic Water (MAW). **b** Map of the seawater neodymium distribution in the Mediterranean Sea based on previous acquired data from stations (violet circles): B, C, 5, 51, 64;⁴⁷ 8, 9, 3, 2,⁴⁹ GeoB7718-3, GeoB7716-1,⁴⁴ 21⁶⁰. **c** Map of the salinity distribution in the Mediterranean Sea based on Medatlas II acquired data.

climate conditions predominated in the E-Med region^{24–26}. Although evidence is inconclusive, some studies have proposed that cold/arid conditions during the YD could have favoured a partial reactivation of the intermediate and/or deep water convection in the E-Med^{13,17,27}.

The maximum reduction of the E-Med intermediate/deep water convection was reached during the early Holocene, with the deposition of an organic-rich sediment layer known as the last Sapropel (S1)^{8,10,13,18,28–32}. General consensus is that the S1 occurred between 10.8 and 6.1 kyr BP³¹, although several authors have proposed that the end of S1 was asynchronous in the water column, with intermediate depths in the E-Med being “re-ventilated” between 7.7 and 7 kyr BP^{33–35}. The S1 formation is attributed to the sum of 1) strong surface ocean stratification resulting from increased influx of fresh-water by river systems, that led to the establishment deep-basin anoxic conditions and 2) increased export productivity resulted in enhanced organic matter fluxes to the deep sea floor^{8,17,31–38}. The potential impact of the S1 in the water exchange between the E- and W-Med sub-basins has also been previously explored^{39–43}. However, no quantitative estimates of changes in the eastern-western water exchange through the Strait of Sicily during the deglacial and Holocene periods are available to date.

In this work we present a continuous record of quantitative estimations of eastern-western water exchange since the last deglaciation, including the YD and the S1 events. Estimations are based on neodymium isotope (ϵ_{Nd}) measurements on planktic foraminifera Fe-Mn crusts, which has been shown to represent well the Nd isotopic signature of the waters masses where foraminifera shells are deposited^{44,45}. Present day E-Med seawater ϵ_{Nd} values are typically higher than W-Med ϵ_{Nd} values (EMDW = -7.1 ± 1.6 $n = 19$, 2σ , LIW = -6.6 ± 1.9 $n = 19$, 2σ , WMDW = -9.1 ± 1.3 ; $n = 12$; 2σ), therefore establishing the basic ground for the use of Nd isotopes as useful tracer of past changes in Med-THC (Fig. 1b)^{44,46–49}.

Gravity core NDT-6-2016 collected during the Next Data expedition (CNR-URANIA R/V, 2016) was recovered at the transition area between the W-Sicily channel and the southern Tyrrhenian Sea ($38^{\circ}0'26,60''$ N and $11^{\circ}47'44,84''$ E) at 1066 m of water depth (Fig. 1a–c). The core depth is below the present-day interphase between WMDW and the EMSW outflowing through the Strait of Sicily, thus a suitable location to evaluate changes in the intermediate-deep water exchange between the two main Mediterranean sub-basins⁴⁹. ϵ_{Nd} results are complemented with other published ϵ_{Nd} records from different regions of the Mediterranean Sea (Fig. 1a)^{39,41,42,50,51}. Through non-linear isotopic end-member modelling we also perform estimates of the mixing proportions between the outflowing EMSW and the WMDW during the late deglaciation and Holocene periods.

Results and discussion

The ϵ_{Nd} record from W-Sicily exhibits remarkable changes along the late deglaciation and Holocene periods (the last ~15 kyr cal. BP). The highest ϵ_{Nd} values are recorded during the YD (between -5.6 ± 0.4 and -6.3 ± 0.3 , 2σ ; Fig. 2), while the lowest ϵ_{Nd} values are predominant during the S1 interval (from -7.8 ± 0.3 to -8.4 ± 0.3 , 2σ ; Fig. 2). The pre-S1 and the post-S1 (between ~11.6 and 10.5 and ~7–6 kyr, respectively)⁵² were characterized by intermediate values ranging from -7.0 ± 0.4 to -7.4 ± 0.6 and from -7.3 ± 0.3 to -7.5 ± 0.3 (2σ), respectively (Fig. 2; Supplementary Table 1). In order to ensure that the measured foraminiferal ϵ_{Nd} values truly reflect changes in the local hydrography without external contributions of Nd coming from terrigenous sediments and/or atmospheric dust deposition^{53–55}, we have conducted additional ϵ_{Nd} analysis in the detrital fraction

< 63 μm . Our lithogenic data show considerably less radiogenic values on the detrital fraction with rather constant values throughout the studied period (from -11.58 ± 0.2 (2σ) to -12.06 ± 0.2 (2σ)) (Supplementary Table 2 and Supplementary Fig. 1). Any potential impact of detrital fraction into the pore water ϵ_{Nd} composition should therefore be expressed as deviations towards more negative ϵ_{Nd} values in the foraminifera samples. Our ϵ_{Nd} results on lithogenic fraction are generally compatible with the ϵ_{Nd} signature of the continental margins at the studied region⁴⁶ and also agree particularly well with a detrital ϵ_{Nd} record from a nearby location at the Gulf of Sirte⁵⁶ (Supplementary Fig. 1). Then, these data, support that our ϵ_{Nd} values obtained from the lithogenic fraction represent well the sedimentological signal of the studied area. Consequently, we can confidently discard any noticeable contribution from terrigenous components because 1) measured lithogenic ϵ_{Nd} is far more unradiogenic (between 4 and 6 ϵ units) than the observed foraminiferal ϵ_{Nd} values obtained in this study and 2) our lithogenic ϵ_{Nd} record shows unchanged values through the studied period and therefore, could not explain the observed changes in our foraminifera ϵ_{Nd} record. We have also discarded any potential Nd remobilization in the sediments induced by oxygen depleted pore waters^{57–59}, since no evidence of sapropel layers and/or low oxygen sediments exist at the W-Sicily record. In addition, the ϵ_{Nd} value of the uppermost sample of the record (Fig. 2, -7.9) is within range of present day seawater ϵ_{Nd} values in the region for depths between 2400 and 400 m, thus, supporting the validity of our results⁶⁰ (Fig. 2b). Nevertheless, although we are confident that contribution of reactive/labile phases from sedimentary sources is negligible, we cannot completely exclude this rare diagenesis process. In this regard, a recent study has shown that to a great extent, the most reactive/labile neodymium is released at the surface ocean, well above the thermocline⁶¹. In addition, an external source of new radiogenic ϵ_{Nd} values during prolonged periods of time should have been recorded elsewhere, but there are no evidences for it in the published records of authigenic or lithogenic neodymium^{39–41,50,62}. These observations provide strong support that our foraminifera ϵ_{Nd} results represent with confidence past seawater ϵ_{Nd} signatures, and thus, the foraminiferal ϵ_{Nd} record from core NDT-6-2016 truly represents changes in the regional oceanography for the last 14 kyr BP.

Enhanced EMSW outflow during the Younger Dryas. The remarkably high ϵ_{Nd} values recorded at the west flank of Sicily channel during the YD are one of the most outstanding features recorded for the studied period (from -5.6 ± 0.4 to -6.3 ± 0.3 , 2σ ; Fig. 2; Supplementary Table 1). We interpret these ϵ_{Nd} values as the result of either or a combination of 1) an enhanced EMSW contribution through the Strait of Sicily into the study area, provided that W-Med sourced waters, such as WMDW, are typically represented by more negative ϵ_{Nd} values (Fig. 2)^{44,46–49}, 2) a shift towards more radiogenic composition in the EMSW end-members, i.e., EMDW and LIW. Since outflowing EMSW comprises a mix between LIW and EMDW⁴⁹, any relative change in the ϵ_{Nd} endmember composition of either of these two water-masses could have also induced variations in the W-Sicily ϵ_{Nd} signature, independently of any changes in the volume of water exported.

This later hypothesis would be in good agreement with previous data from the deep Levantine Sea, showing the presence of a more radiogenic EMDW during the YD than today and attributed to the intensification of Nile river discharge during the African Humid Period (Fig. 2, Nile slope, MS27PT)⁴². Since ϵ_{Nd} values of Nile river sediments range from -7 to 2 ^{46,47}, it is very likely than an increase of river discharge would have favoured the

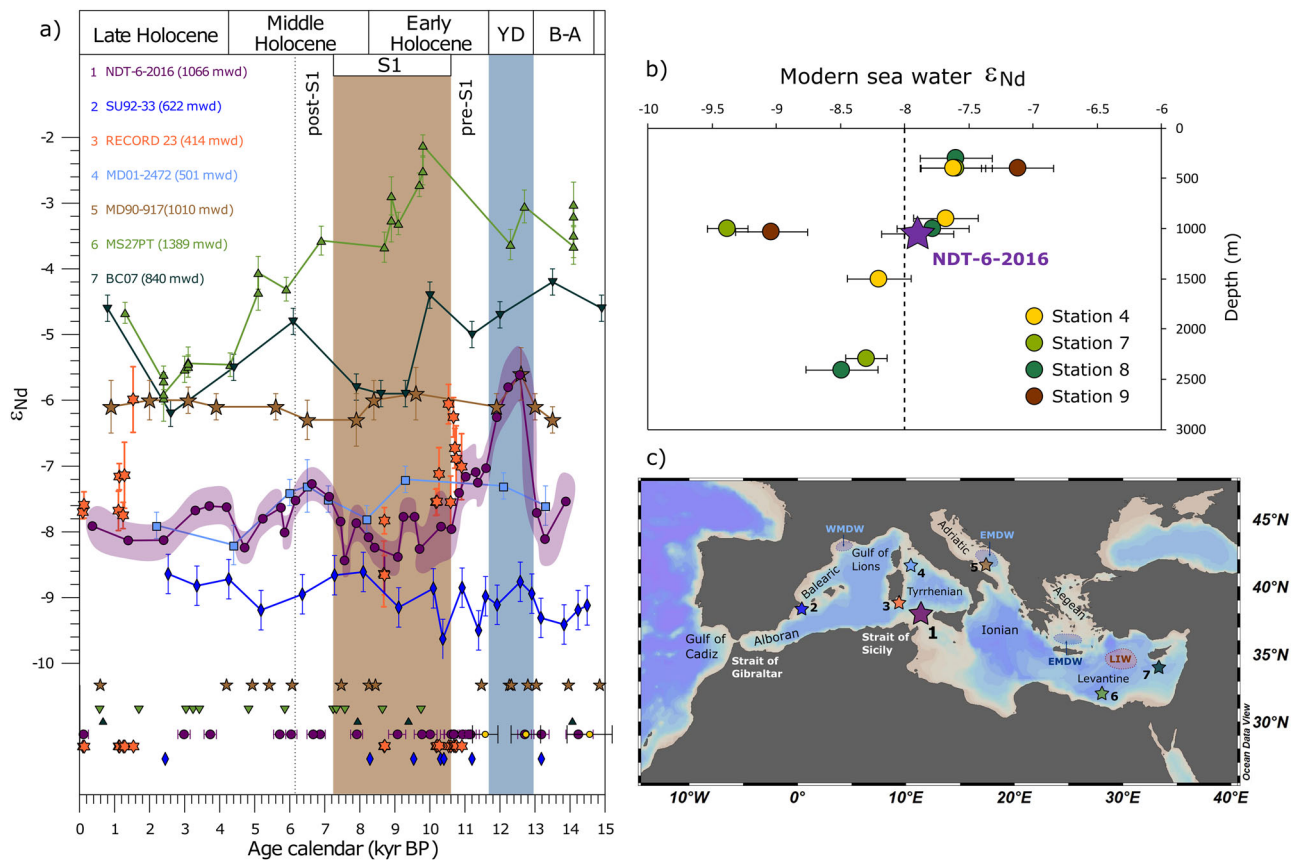


Fig. 2 Neodymium isotopes records from Mediterranean Sea. **a** Records of Neodymium isotopes in planktic foraminifera from NDT-6-2016 (this study), SU92-33 and RECORD23⁴¹, MD01-2472 and MD90-917³⁹, MS27PT⁴² and BC07⁵¹ (violet circles, blue diamonds, orange six pointed stars, light blue squares, brown five pointed stars, light green upward triangles and dark-green downward triangles, respectively). The ^{14}C -calibrated dates used for each chronology are colored according to the corresponding record. In the sediment core NDT-6-2016, violet circles represent ^{14}C -calibrated dates and yellow circles represent tie points. Violet shading correspond to the uncertainties of ϵ_{Nd} results (2sd) of the studied core NDT-6-2016. Error bars reflect the other plotted records uncertainties reported in the bibliography. Grey-blue bar represents YD and light-brown bar, the S1. **b** Modern ϵ_{Nd} seawater values for the Tyrrhenian Sea area⁶⁰ (circles) and ϵ_{Nd} seawater from uppermost sample of NDT-6-2016 (studied core). Dashed line indicate the calculated modern average ϵ_{Nd} seawater value of the Tyrrhenian Sea area through the stations 4, 7, 8, and 9. Error bars reflect uncertainties associated to ϵ_{Nd} results (2sd). **c** Map of the study area in the Mediterranean Sea with the discussed sites location.

formation of higher radiogenic EMDW. In addition, changes in the EMDW ϵ_{Nd} signature could have also been induced through changes in the relative contribution of both Adriatic Sea and Aegean Sea waters to the EMDW. The Adriatic Sea shows relatively constant ϵ_{Nd} values along the studied period (Fig. 2, MD90-917)³⁹, which are consistently more negative than those found in the Levantine Sea (Fig. 2, MS27PT, BC07)^{42,51}. A recent study has shown that modern Aegean Sea water ϵ_{Nd} signature is more positive than Adriatic Sea water ϵ_{Nd} signature (-5.9 ± 0.5 , $n = 6$, 1σ versus -7.4 ± 0.15 , $n = 3$, 1σ , respectively)⁶³, thus increased relative proportions of Aegean/Adriatic waters into the EMDW cannot be discarded as a potential source for the observed YD anomaly. Relatively high ϵ_{Nd} values of EMDW, however, were recorded at the Levantine Sea for the whole deglacial period and early Holocene (Fig. 2)⁴², while at our W-Sicily site the radiogenic ϵ_{Nd} anomaly is restricted to the YD period. Consequently, changes in the EMSW end-member composition cannot solely account for our observations. Nevertheless, despite the generally good correspondence between the W-Sicily ϵ_{Nd} record with an analogous ϵ_{Nd} record from the eastern flank of Corsica, the high ϵ_{Nd} values during the YD at our study site contrast with low ϵ_{Nd} values recorded at Corsica channel (core MD01-2472 in Fig. 2). It is possible that the relatively low temporal resolution of ϵ_{Nd} record from Corsica

could have compromised the identification of this relatively short event. Furthermore, the outflowing EMSW progressively mix with the underlying less radiogenic WMDW, modifying its ϵ_{Nd} signature towards more negative values during its north-westward path⁴⁹. In this scenario it would be reasonable to expect a modified (more negative) ϵ_{Nd} signal at the Corsica site during the YD. Thus, we propose that the ϵ_{Nd} anomaly recorded at our site during the YD likely resulted from the combined effect of 1) the presence of more radiogenic EMSW end-members and 2) the increased contribution of EMSW into the W-Med over this period.

By considering that ϵ_{Nd} values in the W-Sicily site are the result from both changes in EMSW volume export as well as changes in EMSW ϵ_{Nd} end-member composition we present a quantitative estimate of the proportion of EMSW reaching the W-Sicily location through the Strait of Sicily for the studied period. Percentages of EMSW have been estimated applying a simple three endmember isotopic mixing model, using our W-Sicily ϵ_{Nd} record in combination with previously published records as water mass ϵ_{Nd} end-members for WMDW (SU92-33)⁴¹, EMDW (MS27PT)⁴² and LIW (BC07)⁵¹ (Supplementary Table 3)^{41,42,51}.

It must be noted that we used ϵ_{Nd} data from the Levantine Sea as EMDW endmember instead of data from the Adriatic Sea area (Adriatic Deep Water, ADW). As EMDW originates from

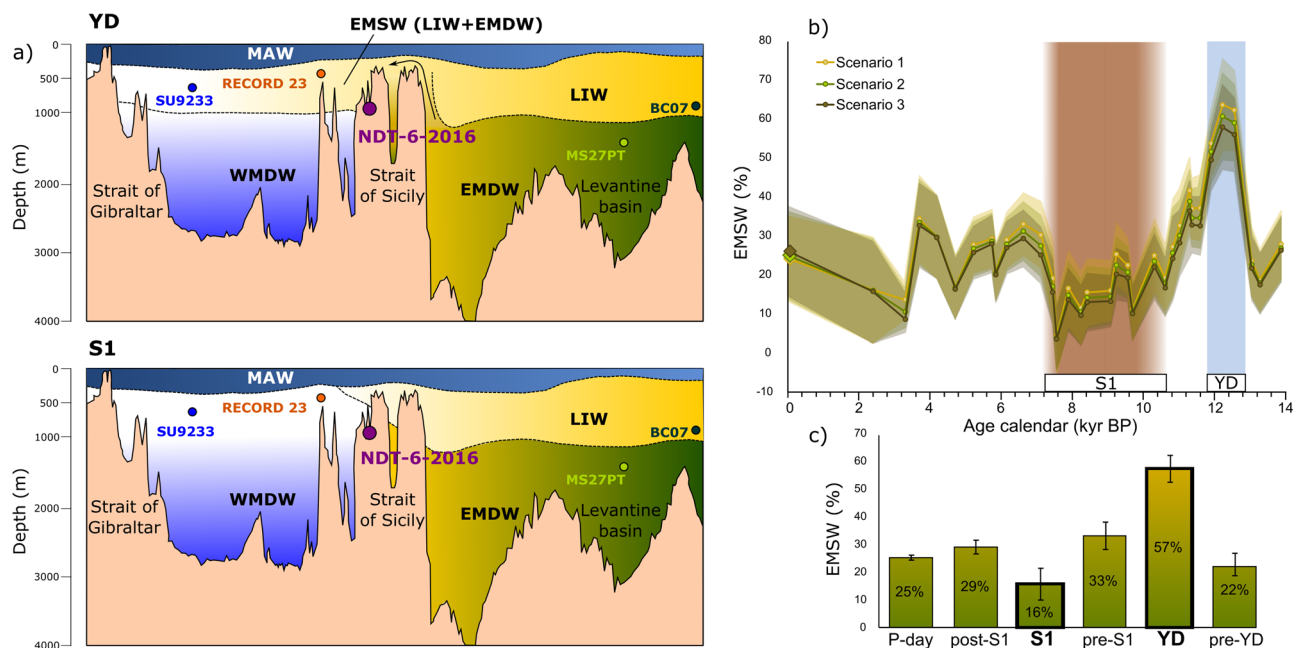


Fig. 3 Water-masses distribution in the Mediterranean Sea. **a** Distribution of intermediate and deep water masses in the Mediterranean Sea during both the YD and S1 and the location of the main cores discussed in this work. **b** Percentages of Eastern Mediterranean Source Water (EMSW) expressed as % contribution. Different scenarios corresponded with different proportions of EMDW and LIW; the first scenario characterized by the same contribution of each water mass, the second one considers a LIW contribution that doubles that of EMDW and the third one takes into account a double contribution of the EMDW with respect to the LIW (yellow, light-green and dark-green lines, respectively). Shading represents the range of uncertainty in the reconstruction (95%), based on analytical errors. Grey-blue bar represents the YD and light-brown bar the S1. Current percentages of EMSW are calculated using present-day seawater ϵ_{Nd} values from WMDW, LIW, EMDW⁴⁷ and South Tyrrhenian Sea⁴⁹ and are indicated with rhombs (see supplementary Table 3). **c** Average values of EMSW export in the studied location for each period discussed in this work. Error bars reflect the uncertainties associated to the average values calculated for each period (YD, $n = 9$; pre-YD, $n = 9$; post-YD, $n = 15$; S1, $n = 33$; 2sd). Error bar for present-day values correspond to the uncertainty in the reconstruction (95%), based on analytical errors.

different mixing proportions of both Aegean and Adriatic waters, using ADW alone as the EMDW endmember would not be an accurate representation of this water mass^{2,4}. In order to account for the uncertainties associated with mixing estimates as well as intrinsic analytical errors in our and previously published Nd isotope ratios, we have implemented a Monte-Carlo approach of the mixing equation (see details in methods section). Furthermore, since proportions of LIW and EMDW contributing to the EMSW in the past are unknown, different scenarios in the relative mixing proportions between LIW and EMDW have been considered (LIW = EMDW, LIW = 2*EMDW, and EMDW = 2*LIW; see details in methods section). Previous calculations of EMSW proportions using potential temperature, salinity and oxygen (20–40%)⁴⁹ agree with our present-day estimations of EMSW contribution at W-Sicily (~30%; Fig. 3), thus, supporting the robustness of the mixing model.

Mixing estimates calculations further support a larger proportion of EMSWs arriving into W-Sicily during the YD (Fig. 3b, c), as compared to the pre- and post-YD (in average: YD, $57 \pm 5\%$, $n = 9$; pre-YD, $23 \pm 4\%$, $n = 9$; post-YD, $33 \pm 5\%$, $n = 15$; Fig. 3a–c). Our mixing estimates are supported by previous results from an ocean-biogeochemical model experiment and proxy compilation¹⁷, that show a partial re-ventilation of the E-Med basin during the YD. This situation could be associated with increased cooling and aridity conditions in the Aegean Sea that could have favoured an intense deep water convection in the area (Fig. 4g)^{24,25}. Enhanced deep water convection in the Aegean Sea during the YD is also coherent with the higher ϵ_{Nd} values recorded in W-Sicily.

Interestingly, the higher ϵ_{Nd} values recorded during the YD at our site are in direct concurrence with maximum values in

sediment grain-size reported from both a shallower and distal core located at the eastern flank of Corsica (at 501 mwd, Fig. 4e)¹³ and also from an even further west and deeper core in the Alboran Sea (at 914 mwd, Fig. 4d)⁶⁴. These grain size records suggest an increase in the currents velocity at intermediate depths in the W-Med during the YD, that is also synchronous with increased speed of Mediterranean waters outflowing the Strait of Gibraltar as reported in contourite deposits of the Gulf of Cadiz^{6,65,66} (Fig. 4a), suggesting a direct connection between the EMSW flow and MOW. In addition, enhanced YD EMSW outflow occurred simultaneously with the arrival of more oxygenated waters at intermediate depths in the Alboran Sea (Fig. 4c), whereas the deep basin was characterized by poorly-oxygenated conditions as a result of weakened W-Med deep water convection at this time (Fig. 4b)⁶⁷. We hypothesize that enhanced YD EMSW outflow 1) could have induced changes in the W-Med deep-water convection that led to a re-oxygenation at intermediate depths (~900 m) and 2) could also be linked to the intensification of MOW currents through the Strait Gibraltar⁶.

Weakening in the westward flow of Eastern Mediterranean Source Waters during the last Sapropel.

In contrast to the high ϵ_{Nd} values described during the YD in our W-Sicily record, our results show that the S1 period is identified by relatively low ϵ_{Nd} values, (Fig. 2; from -8.4 ± 0.3 to -7.8 ± 0.3 , 2 σ), i.e., between ~2 and 3-unit lower than for the YD period (between -5.6 ± 0.4 and -6.3 ± 0.3 , 2 σ). This relatively low ϵ_{Nd} values are interpreted as a response of a weaker outflow of EMSW into the W-Sicily during the S1 (Fig. 3a). This interpretation is supported by the low percentages of EMSW obtained throughout the end-member

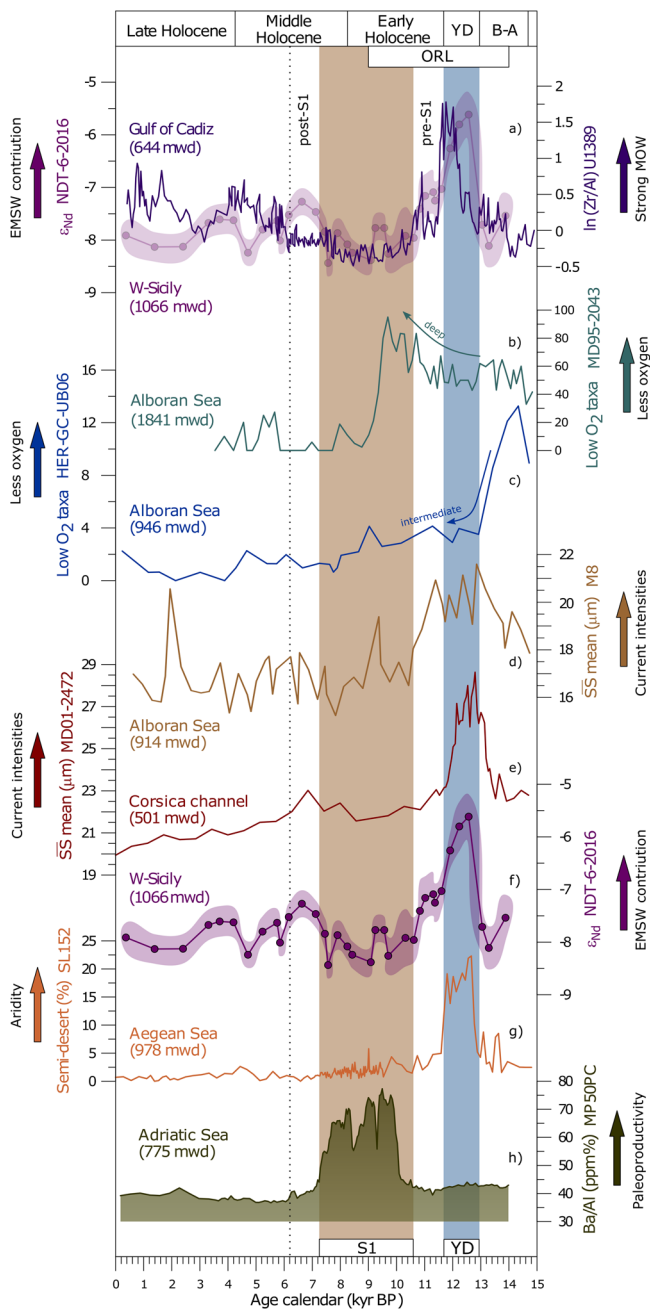


Fig. 4 Comparison between marine records from the Mediterranean region. From the top to the base: **(a)** Zr/Al from U139⁶, **b, c** Low oxygen benthic foraminiferal taxa percentages from intermediate record HER-GC-UB6 and deep MD95-2043⁶⁷ respectively. **d, e** Grain-size measurements from M8⁶⁴ and MD01-2472⁸⁷ respectively. **f** Neodymium isotope records from NDT-6-2016 (this study). **g** Semi-desert taxa percentages obtained from SL152^{24,88}. **h** Ba/Al profiles from MP50PC³⁴. Grey-blue bar represents the YD and light-brown bar the S1.

mixing model estimates (in average: $16 \pm 6\%$, $n = 33$; Fig. 3b, c), i.e., approximately one half of EMSW exports estimated for the pre- and post-S1 (in average: pre-S1, $33 \pm 5\%$, $n = 15$; post-S1, $29 \pm 2\%$, $n = 9$; Fig. 3b, c).

Our relative low ϵ_{Nd} values recorded at W-Sicily also agree with previous ϵ_{Nd} results from the Sardinia channel measured in deep-sea corals at 414 m, both of them showing a decrease in the ϵ_{Nd} records from the pre-S1 to the S1 (Fig. 2)⁴¹. Thus, ϵ_{Nd} data from both W-Sicily and Sardinia channel support moderate EMSW

outflow during the pre-S1 but, particularly show an important reduction in the export during the S1 period at both locations. All these indicators are consistent with a weaker EMSW outflow during the S1, which presumably resulted in a larger volume of low ϵ_{Nd} WMDW occupying intermediate depths at the study site (Fig. 3a). The end of the S1 period is shown as a transition in the ϵ_{Nd} values from -8.4 ± 0.3 to -7.5 ± 0.3 units (2σ) (Fig. 2). Quantitative mixing estimates indicate that this transition accounted for an increase in the EMSW contribution from $4 \pm 8\%$ to $28 \pm 8\%$ at the W-Sicily (Fig. 3b). These results confirm an increase in the export of EMSW through the Strait of Sicily at the end of the S1, likely indicating the end of the deep water stagnant conditions that prevailed in the E-Med during the S1 interval. Interestingly, the estimated decrease in the EMSW outflow agrees well with an intense weakening of MOW current intensities (Fig. 4e) described at the Gulf of Cadiz^{6,65,66}. This situation supports the previously argued control of E-Med intermediate/deep water convection on the MOW intensities and its impact in the Atlantic Meridional Overturning Circulation^{7,68}.

The end of the S1 stagnation occurred between 7.5 and 7 kyr BP according to our age model⁵², suggesting that the interconnection between the E-W Mediterranean basins was re-established ~ 1 kyr before the end of the S1 period around 6.1 kyr BP³¹. If this observation was confirmed, it would support that the re-activation of intermediate and deep water circulation might have not occurred synchronously across the E-Med basin, but instead, intermediate waters would have been re-ventilated before any other deeper water masses in the basin. This hypothesis is coherent with previous evidences for an earlier S1 re-ventilation between 7.7 and 7 kyr BP, both in the Adriatic and the Aegean Sea (Fig. 4h)^{34,35,38,69,70}. Although this earlier re-ventilation at intermediate depths might have not affected the deep basin, our records indicate that it would have been strong enough to re-establish the intense water exchange between the E-Med and W-Med.

Summary and conclusions. ϵ_{Nd} data from sediment core NDT-6-2016 at 1066 m provide quantitative information on the proportion of EMSW exported towards the W-Med basin, during the last deglacial/Holocene periods. The highest percentages of EMSW are identified at W-Sicily during the YD ($57 \pm 5\%$) indicating that an enhanced intermediate-deep water interconnection prevailed between the E-Med and the W-Med. We speculate that this situation responded to the combined effect of enhanced convection in the Aegean and Levantine basins in response to a regional aridification phase and a weaker western deep water formation that led to a deeper expansion of the EMSW into the western basin. We propose that enhanced westward flow of EMSW also corresponds with the previously described stronger currents at intermediate depths of the W-Med. This situation would have induced changes in the W-Med deep water convection promoting re-oxygenation of intermediate layers (~ 900 m) and ceasing the stagnation initiated during the last Organic Rich layer formation in the westernmost part of the Mediterranean Sea. Estimated proportions of EMSW for the S1 period provide the minimum values of the record ($16 \pm 6\%$), supporting a substantial reduction of the EMSW outflow through the Strait of Sicily. We propose that the outflow of EMSW through the Strait of Sicily at 7.5 and 7 kyr BP is related to an earlier convection enhancement in the Adriatic and Aegean Seas, that marked the end of the stagnant conditions at intermediate depths of the E-Med. The described evolution of EMSW flow at W-Sicily, vigorous during the YD and weak during the S1, agrees well with changes in MOW current intensities at the Gulf of Cadiz. These

results highlight the relevance of the E-Med intermediate/deep water convection in controlling the intensity of MOW.

Materials and Methods

Core description. The gravity core NDT-6-2016 (~4 m long) was sampled every cm and consists of homogeneous silty-clay sediments with no sedimentary irregularities along the whole sequence. Neodymium isotopes were analysed every 2–6 cm for the interval between 1.20 and 1.62 m and at lower resolution (10–30 cm) for the rest of the core.

$$\epsilon_{Nd_{mix}} = \frac{(\epsilon_{Nd_{WMDW}} * [Nd]_{WMDW} * f_{WMDW}) + (\epsilon_{Nd_{LIW}} * [Nd]_{LIW} * f_{LIW}) + (\epsilon_{Nd_{EMDW}} * [Nd]_{EMDW} * f_{EMDW})}{([Nd]_{WMDW} * f_{WMDW}) + ([Nd]_{LIW} * f_{LIW}) + ([Nd]_{EMDW} * f_{EMDW})} \quad (1)$$

Radiocarbon dates and age model. The chronological framework was established by twenty ^{14}C dates analysed in monospecific planktic foraminifera samples (> 250 μm , *Globoconella inflata*). Radiocarbon ages were calibrated using MARINE20 calibration⁷¹. In addition to the ^{14}C dates of the lower part, three tie points were added based on an adjusted alignment between the studied $\delta^{18}O$ record from *Globigerina bulloides* and the well-dated reference NGRIP isotope record^{72,73}. The age model⁵² was constructed using the Bayesian statistics software Bacon⁷⁴.

Neodymium isotope measurements. A total of 32 samples were selected for neodymium isotope analyses. For each sample, 20 to 30 mg of mixed planktic foraminifera from the > 212 μm fraction were handpicked, except for those samples where planktic foraminifera were scarce and only 4 to 12 mg were available. Each sample was processed individually and the specimens were crushed with extreme care to avoid the over-crushing using two glass slides under the microscope. Each sample was cleaned with Ultra-Pure water (Resistivity > 18 M Ω cm) as many times as necessary to remove the clay fraction, and then rinsed with methanol to eliminate particles that could have remained attached to the vial^{75,76}. Between each Ultra-Pure water and methanol cleanings, samples were sonicated to re-suspend the clay fraction. Sample dissolution was carried out by adding 0.5 ml of Ultra-Pure water and 0.1 ml of acetic acid in each sample. Then, they were sonicated until completely dissolved. Finally, all samples were centrifuged to avoid possible undissolved particles and transferred to clean vials to carry out the sample purification. In addition, Nd isotope ratios were measured on five bulk sediment samples on the < 63 μm size fraction. Around 150 mg of dry sediment samples was taken and grinded to obtain a very fine dust. In order to extract the detrital component in the bulk sediments a sequential leaching protocol was applied⁷⁷. Leaching steps consisted in 1) organic matter removal, 2) carbonate leaching and 3) authigenic components removal. After these steps, digestion of detrital samples was performed following⁷⁸. Samples for Nd isotope analysis on foraminifera coatings and terrigenous fraction (< 63 μm) were treated and purified by standard column chromatography methods at the Laboratori d'Isòtops Radiogenics i Ambientals (LIRA) of the Universitat de Barcelona (UB). In the case of foraminifera coatings chromatography consisted in two steps⁷⁹; 1) rare elements (REE) were separated from sample matrix and collected using a Tru-spec resin chemistry and 2) neodymium was isolated from other REE by means of the Ln-Spec resin chromatography. For terrigenous fraction we followed an elution procedure in a controlled-pressured vacuum system⁸⁰. Measurements of ϵ_{Nd} were performed using a Plasma 3 Multi Collector Inductively Coupled Plasma Mass Spectrometer (Nu Instruments-AMETEK) at Centres Científics i Tecnològics of the Universitat de Barcelona (CCiTUB). Procedural blanks were systematically corrected and were always found to be negligible (between 26 and 45 pg of Nd). The $^{143}Nd/^{144}Nd$ instrumental mass bias was corrected using the exponential law⁸¹, assuming a reference $^{146}Nd/^{144}Nd$ ratio of 0.7219. Furthermore, the JNdi-1 standard was analysed before and after each sample, and an additional sample-standard bracketing normalization of the mass bias corrected ratios was carried out, using the reference $^{143}Nd/^{144}Nd$ value of 0.512115 ± 0.000007 for this standard⁸². Nd isotopic composition is expressed as $\epsilon_{Nd} = ((^{143}Nd/^{144}Nd)_{sample}/(^{143}Nd/^{144}Nd)_{CHUR} - 1) * 10^4$, where CHUR is the Chondritic Uniform Reservoir and represents a present-day Earth value of $(^{143}Nd/^{144}Nd)_{CHUR} = 0.512638$ ⁸³. Uncertainties of the ϵ_{Nd} values correspond to the external reproducibility of the JNdi-1 analysis performed throughout each measurement session (2sd, $n = 12-20$), except for samples with internal standard error larger than 2sd. Uncertainties ranged between 0.3 and 0.5 ϵ_{Nd} -units, depending on the Nd amounts in the samples. The accuracy of the method has been demonstrated through multiple analysis of the AMES II standard (0.511972 ± 0.000012 , 2 SD = 23 ppm, $n = 79$), and results were not significantly from those previously published⁸⁴⁻⁸⁶. In addition, 4 independently replicated sample analysis have been conducted at core depth "147 cm", from foraminifera picking, cleaning, sample purification and analysis. Our replicated sample results range from -7.7 to -8.0 (mean $\epsilon_{Nd} = -7.8 \pm 0.3$, $n = 4$; 2 σ), with a standard error of ± 0.2 (Supplementary Table 4).

Estimation of water masses mixing using Nd isotopes. Water mass mixing estimations were performed using our W-Sicily ϵ_{Nd} record in combination with three previously published W- and E-Med ϵ_{Nd} records. Isotopic mixing equations require previous knowledge on the isotopic composition (as well as elemental abundance) of the different end-members considered. In the case of water masses mixing in the ocean, it is also necessary to consider time-evolving end-member Nd isotope composition into the mixing model. For this reason, in this work we have defined the Nd end-member composition based on existing ϵ_{Nd} records in the area of study from sediment core SU92-33 (WMDW), MS27PT (EMDW) and BC07 (LIW)^{41,42,51}. The estimates of EMSW export were carried out according to the following equation:

where $\epsilon_{Nd_{mix}}$ correspond to our measured ϵ_{Nd} values from core NDT-6-2016, whereas $\epsilon_{Nd_{WMDW}}$, $\epsilon_{Nd_{LIW}}$, $\epsilon_{Nd_{EMDW}}$ are the ϵ_{Nd} values from cores SU92-33, MSPT2 and BC07 respectively. $[Nd]$ corresponds to the neodymium concentration of WMDW, EMDW as well as LIW and f is the relative proportion of each water-mass, according to the mixing mass balance constraint that $f_1 + f_2 + f_3 = 1$ (Fig. 3a). In order to overcome heterogeneous age sampling among the different records utilized we have performed linear interpolation in the ϵ_{Nd} values from cores SU92-33, BC07, and MS27PT to match the ages samples at our study site (Supplementary Table 3). Unfortunately, there is no way to estimate reliably past seawater Nd concentrations to date. Thus, to account for the uncertainties derived from the lack of reliable past-seawater Nd concentration estimates as well as to account for analytical uncertainties, we have implemented a Monte-Carlo approach of the mixing equation. The Monte-Carlo approach estimates the most likely resulting scenarios from a set of 10,000 simulations of the mixing equation using pseudo-random number generation for every single variable considered. This means random numbers within the 2 σ analytical uncertainty for each Nd isotope value considered at the 4 core sites. For the Nd concentrations we have considered typical uncertainties in present day seawater measurements of Nd concentrations (see below). The dataset resulting from running 10,000 simulations is then assessed statistically, and the mean values and standard error values are obtained for the different mixing proportions estimated. As a work around to the problem of having 3 unknowns with 2 equations we have considered different scenarios in the mixing proportions between the eastern Mediterranean water masses contributing to the EMSW, i.e., LIW and EMDW. The first scenario is defined by the same relative contribution of LIW and EMDW (i.e. $f_{LIW} = f_{EMDW}$), the second scenario the contribution of the LIW doubles that of the EMDW (i.e., $f_{LIW} = 2 * f_{EMDW}$) and the third scenario considers that the proportion of EMDW doubles that of the LIW (i.e. $f_{EMDW} = 2 * f_{LIW}$) (Supplementary Table 5). Nd concentrations used for WMDW, LIW and EMDW have been 23.05 ± 1.05 , 27.8 ± 1.6 , and 28.25 ± 3.35 respectively, based on present-day Nd concentrations measured in each water-mass⁴⁷.

Data availability

All data of neodymium isotopes from the studied core NDT-6-2016 is available in the NOAA/NCEI paleo data repository (<https://www.nccei.noaa.gov/access/paleo-search/study/37726>).

Received: 3 July 2022; Accepted: 17 April 2023;

Published online: 29 April 2023

References

1. Millot, C. Circulation in the hydrodynamics general circulation mediterranean sea Mesoscale phenomena. *Oceanol. Acta* **10**, 143–149 (1987).
2. Millot, C. Circulation in the Western Mediterranean Sea. *J. Mar. Syst.* **20**, 423–442 (1999).
3. Pinardi, N. & Masetti, E. Variability of the large scale general circulation of the Mediterranean Sea from observations and modelling: A review. *Palaeoogeogr. Palaoclimatol. Palaeoecol.* **158**, 153–173 (2000).
4. Lascaratos, A., Williams, R. G. & Tragou, E. A mixed-layer study of the formation of Levantine Intermediate Water. *J. Geophys. Res.* **98**, 14739–14749 (1993).
5. Voelker, A. H. L. et al. Mediterranean outflow strengthening during northern hemisphere coolings: A salt source for the glacial Atlantic? *Earth Planet. Sci. Lett.* **245**, 39–55 (2006).
6. Bahr, A. et al. Persistent monsoonal forcing of mediterranean outflow water dynamics during the late Pleistocene. *Geology* **43**, 951–954 (2015).

7. Swingedouw, D., Colin, C., Eynaud, F., Ayache, M. & Zaragosi, S. Impact of freshwater release in the Mediterranean Sea on the North Atlantic climate. *Clim. Dyn.* **53**, 3893–3915 (2019).
8. Rohling, E. J., Marino, G. & Grant, K. M. Mediterranean climate and oceanography, and the periodic development of anoxic events (sapropels). *Earth-Science Rev.* **143**, 62–97 (2015).
9. Cacho, I. et al. Variability of the western Mediterranean Sea surface temperature during the last 25,000 years and its connection with the northern hemisphere climatic changes. *Clim. Chang.* **16**, 40–52 (2001).
10. Schmiel, G. et al. Climatic forcing of eastern Mediterranean deep-water formation and benthic ecosystems during the past 22 000 years. *Quat. Sci. Rev.* **29**, 3006–3020 (2010).
11. Frigola, J. et al. Evidence of abrupt changes in Western Mediterranean Deep Water circulation during the last 50 kyr: A high-resolution marine record from the Balearic Sea. *Quat. Int.* **181**, 88–104 (2008).
12. Rogerson, M. et al. A dynamic explanation for the origin of the western Mediterranean organic-rich layers. *Geochem. Geophys. Geosys.* **9**, 1–20 (2008).
13. Toucanne, S. et al. Tracking rainfall in the northern Mediterranean borderlands during sapropel deposition. *Quat. Sci. Rev.* **129**, 178–195 (2015).
14. Revel, M. et al. 20,000 years of Nile River dynamics and environmental changes in the Nile catchment area as inferred from Nile upper continental slope sediments. *Quat. Sci. Rev.* **130**, 200–221 (2015).
15. Coulthard, T. J., Ramirez, J. A., Barton, N., Rogerson, M. & Brücher, T. Were rivers flowing across the Sahara during the last interglacial? Implications for human migration through Africa. *PLoS One* **8**, e74834 (2013).
16. Wu, J. et al. North-African paleodrainage discharges to the central Mediterranean during the last 18,000 years: A multiproxy characterization. *Quat. Sci. Rev.* **163**, 95–113 (2017).
17. Grimm, R. et al. Late glacial initiation of Holocene eastern Mediterranean sapropel formation. *Nat. Commun.* **6**, 7099 (2015).
18. Grant, K. M. et al. The timing of Mediterranean sapropel deposition relative to insolation, sea-level and African monsoon changes. *Quat. Sci. Rev.* **140**, 125–141 (2016).
19. Tierney, J. E., Pausata, F. S. R. & Peter, B. Rainfall regimes of the Green Sahara. *Sci. Adv.* **3**, e1601503 (2017).
20. DeMenocal, P. et al. Abrupt onset and termination of the African Humid Period: Rapid climate responses to gradual insolation forcing. *Quat. Sci. Rev.* **19**, 347–361 (2000).
21. Mohtadi, M., Prange, M. & Steinke, S. Palaeoclimatic insights into forcing and response of monsoon rainfall. *Nature* **533**, 191–199 (2016).
22. Shanahan, T. M. et al. The time-transgressive termination of the African humid period. *Nat. Geosci.* **8**, 140–144 (2015).
23. Ménot, G. et al. Timing and stepwise transitions of the African Humid Period from geochemical proxies in the Nile deep-sea fan sediments. *Quat. Sci. Rev.* **228**, 106071 (2020).
24. Dormoy, I. et al. Terrestrial climate variability and seasonality changes in the Mediterranean region between 15000 and 4000 years BP deduced from marine pollen records. *Clim. Past* **5**, 615–632 (2009).
25. Kotthoff, U. et al. Impact of Lateglacial cold events on the northern Aegean region reconstructed from marine and terrestrial proxy data. *J. Quat. Sci.* **26**, 86–96 (2011).
26. Gasse, F. Hydrological changes in the African tropics since the last Glacial maximum. *Rev. Quat. Sci.* **19**, 189–211 (2000).
27. McCulloch, M. et al. Proliferation and demise of deep-sea corals in the Mediterranean during the younger dryas. *Earth Planet. Sci. Lett.* **298**, 143–152 (2010).
28. Rossignol-Strick, M. Mediterranean Quaternary sapropels, an immediate response of the African monsoon to variation of insolation. *Palaeogeogr. Palaeoclimatol. Palaeoecol.* **49**, 237–263 (1985).
29. Lourens, L. J., Hilgen, F. J., Gudjonsson, L. & Zachariasse, W. J. Late Pliocene to early Pleistocene astronomically forced sea surface productivity and temperature variations in the Mediterranean. *Mar. Micropaleontol.* **19**, 49–78 (1992).
30. Rohling, E. J. Review and new aspects concerning the formation of eastern Mediterranean sapropels. *Mar. Geol.* **122**, 1–28 (1994).
31. De Lange, G. J. et al. Synchronous basin-wide formation and redox-controlled preservation of a Mediterranean sapropel. *Nat. Geosci.* **1**, 606–610 (2008).
32. Mercone, D., Thomson, J., Abu-Zied, R. H., Croudace, I. W. & Rohling, E. J. High-resolution geochemical and micropaleontological profiling of the most recent eastern Mediterranean sapropel. *Mar. Geol.* **177**, 25–44 (2001).
33. Tesi, T. et al. Large-scale response of the Eastern Mediterranean thermohaline circulation to African monsoon intensification during sapropel S1 formation. *Quat. Sci. Rev.* **159**, 139–154 (2017).
34. Filippidi, A., Triantaphyllou, M. V. & De Lange, G. J. Eastern-Mediterranean ventilation variability during sapropel S1 formation, evaluated at two sites influenced by deep-water formation from Adriatic and Aegean Seas. *Quat. Sci. Rev.* **144**, 95–106 (2016).
35. Checa, H. et al. High resolution paleo-environmental changes during the Sapropel 1 in the North Ionian Sea, central Mediterranean. *The Holocene* **30**, 1–12 (2020).
36. Bianchi, D. et al. Simulations of ecosystem response during the sapropel S1 deposition event. *Palaeogeogr. Palaeoclimatol. Palaeoecol.* **235**, 265–287 (2006).
37. Revel, M. et al. 21,000 Years of Ethiopian African monsoon variability recorded in sediments of the western Nile deep-sea fan. *Reg. Environ. Chang.* **14**, 1685–1696 (2014).
38. Incarbona, A., Abu-Zied, R. H., Rohling, E. J. & Ziveri, P. Reventilation episodes during the Sapropel S1 deposition in the eastern Mediterranean based on Holococcolith preservation paleoceanography and paleoclimatology. *Paleoceanogr. Paleoclimatol.* **34**, 1–13 (2019).
39. Colin, C. et al. Changes in the intermediate water masses of the Mediterranean sea during the last climatic cycle—New constraints from Neodymium Isotopes in Foraminifera. *Paleoceanogr. Paleoclimatol.* **36**, 1–28 (2021).
40. Cornuault, M. et al. Circulation changes in the Eastern Mediterranean Sea Over the Past 23,000 Years inferred from authigenic Nd isotopic ratios. *Paleoceanogr. Paleoclimatol.* **33**, 264–280 (2018).
41. Dubois-Dauphin, Q. et al. Hydrological variations of the intermediate water masses of the western Mediterranean Sea during the past 20 ka inferred from neodymium isotopic composition in foraminifera and cold-water corals. *Clim. Past* **13**, 17–37 (2017).
42. Duhamel, M. et al. Variations in eastern Mediterranean hydrology during the last climatic cycle as inferred from neodymium isotopes in foraminifera. *Quat. Sci. Rev.* **237**, 106306 (2020).
43. Murat, A. Pliocene – Pleistocene occurrence of sapropels in the western Mediterranean Sea and their relation to eastern Mediterranean sapropels. *Proc. Ocean Drill. Program, Sci. Results* **161**, 519–527 (1999).
44. Vance, D. et al. The use of foraminifera as a record of the past neodymium isotope composition of seawater. *Paleoceanography* **19**, 1–17 (2009).
45. Tachikawa, K., Piotrowski, A. M. & Bayon, G. Neodymium associated with foraminiferal carbonate as a recorder of seawater isotopic signatures. *Quat. Sci. Rev.* **88**, 1–13 (2014).
46. Ayache, M. et al. High-resolution neodymium characterization along the Mediterranean margins and modelling of Nd distribution in the Mediterranean basins. *Biogeosciences* **13**, 5259–5276 (2016).
47. Tachikawa, K. et al. Neodymium isotopes in the Mediterranean Sea: Comparison between seawater and sediment signals. *Geochim. Cosmochim. Acta* **68**, 3095–3106 (2004).
48. Henry, F., Jeandel, C., Dupré, B. & Minster, J. F. Particulate and dissolved Nd in the western Mediterranean Sea: Sources, fate and budget. *Mar. Chem.* **45**, 283–305 (1994).
49. Garcia-Solsona, E. et al. Rare earth elements and Nd isotopes as tracers of modern ocean circulation in the central Mediterranean Sea. *Prog. Oceanogr.* **185**, 102340 (2020).
50. Wu, J. et al. Divergent Mediterranean seawater circulation during Holocene sapropel formation – Reconstructed using Nd isotopes in fish debris and foraminifera. *Earth Planet. Sci. Lett.* **511**, 141–153 (2019).
51. Freyrier, R., Michard, A., De Lange, G. & Thomson, J. Nd isotopic compositions of Eastern Mediterranean sediments: Tracers of the Nile influence during sapropel S1 formation? *Mar. Geol.* **177**, 45–62 (2001).
52. Trias-Navarro, S. et al. Surface hydrographic changes at the western flank of the Sicily Channel associated with the last sapropel. *Glob. Planet. Change* **204**, 103582 (2021).
53. Arsouze, T., Dutay, J. C., Lacan, F. & Jeandel, C. Modeling the neodymium isotopic composition with a global ocean circulation model. *Chem. Geol.* **239**, 165–177 (2007).
54. Rempfer, J., Stocker, T. F., Joos, F., Dutay, J. C. & Siddall, M. Modelling Nd-isotopes with a coarse resolution ocean circulation model: Sensitivities to model parameters and source/sink distributions. *Geochim. Cosmochim. Acta* **75**, 5927–5950 (2011).
55. Siddall, M. et al. Towards explaining the Nd paradox using reversible scavenging in an ocean general circulation model. *Earth Planet. Sci. Lett.* **274**, 448–461 (2008).
56. Blanchet, C. L. et al. Drivers of river reactivation in North Africa during the last glacial cycle. *Nat. Geosci.* **14**, 97–103 (2021).
57. Wilson, D. J., Piotrowski, A. M., Galy, A. & Clegg, J. A. Reactivity of neodymium carriers in deep sea sediments: Implications for boundary exchange and paleoceanography. *Geochim. Cosmochim. Acta* **109**, 197–221 (2013).
58. Du, J. et al. Reactive-transport modeling of neodymium and its radiogenic isotope in deep-sea sediments: The roles of authigenesis, marine silicate weathering and reverse weathering. *Earth Planet. Sci. Lett.* **596**, 117792 (2022).
59. Skinner, L. C. et al. Rare Earth Elements in early-diagenetic foraminifer ‘coatings’: Pore-water controls and potential paleoceanographic applications. *Geochim. Cosmochim. Acta* **245**, 118–132 (2019).

60. Garcia-Solsona, E. & Jeandel, C. Balancing rare earth element distributions in the northwestern Mediterranean sea. *Chem. Geol.* **532**, 119372 (2020).
61. Wu, Y. et al. Assessing neodymium isotopes as an ocean circulation tracer in the Southwest Atlantic. *Earth Planet. Sci. Lett.* **599**, 117846 (2022).
62. Jiménez-Espejo, F. J. et al. Geochemical evidence for intermediate water circulation in the westernmost Mediterranean over the last 20 kyr BP and its impact on the Mediterranean Outflow. *Glob. Planet. Change* **135**, 38–46 (2015).
63. Montagna, P. et al. Dissolved neodymium isotopes in the Mediterranean Sea. *Geochim. Cosmochim. Acta* **322**, 143–169 (2022).
64. Alonso, B. et al. Paleoceanographic and paleoclimatic variability in the Western Mediterranean during the last 25 cal. kyr BP. New insights from contourite drifts. *Mar. Geol.* **437**, 106488 (2021).
65. Lebreiro, S. M., Antón, L., Reguera, M. I. & Marzocchi, A. Paleoceanographic and climatic implications of a new Mediterranean Outflow branch in the southern Gulf of Cadiz. *Quat. Sci. Rev.* **197**, 92–111 (2018).
66. Sierro, F. J. et al. Mediterranean Overflow Over the Last 250 kyr: Freshwater Forcing From the Tropics to the Ice Sheets. *Paleoceanogr. Paleoclimatology* **35**, 1–31 (2020).
67. Pérez-Asensio, J. N. et al. Changes in western Mediterranean thermohaline circulation in association with a deglacial Organic Rich Layer formation in the Alboran Sea. *Quat. Sci. Rev.* **228**, 106075 (2020).
68. Ivanovic, R. F., Valdes, P. J., Gregoire, L., Flecker, R. & Gutjahr, M. Sensitivity of modern climate to the presence, strength and salinity of Mediterranean-Atlantic exchange in a global general circulation model. *Clim. Dyn.* **42**, 859–877 (2014).
69. Siani, G., Magny, M., Paterne, M., Debret, M. & Fontugne, M. Paleohydrology reconstruction and Holocene climate variability in the South Adriatic Sea. *Clim. Past* **9**, 499–515 (2013).
70. Cascella, A. et al. The response of calcareous plankton to the Sapropel S1 interval in North Ionian Sea. *Glob. Planet. Change* **205**, 103599 (2021).
71. Heaton, T. J. et al. Marine20 - The Marine Radiocarbon Age Calibration Curve (0–55,000 cal BP). *Radiocarbon* **62**, 779–820 (2020).
72. Vinther, B. M. et al. A synchronized dating of three Greenland ice cores throughout the Holocene. *J. Geophys. Res. Atmos.* **111**, 1–11 (2006).
73. Rasmussen, S. O. et al. A new Greenland ice core chronology for the last glacial termination. *J. Geophys. Res. Atmos.* **111**, 1–16 (2006).
74. Blaauw, M. & Christeny, J. A. Flexible paleoclimate age-depth models using an autoregressive gamma process. *Bayesian Anal.* **6**, 457–474 (2011).
75. Barker, S., Greaves, M. & Elderfield, H. A study of cleaning procedures used for foraminiferal Mg/Ca paleothermometry. *Geochemistry, Geophys. Geosystems* **4**, 1–20 (2003).
76. Pena, L. D., Calvo, E., Cacho, I., Eggins, S. & Pelejero, C. Identification and removal of Mn-Mg-rich contaminant phases on foraminiferal tests: Implications for Mg/Ca past temperature reconstructions. *Geochem. Geophys. Geosystems* **6**, Q09P02 (2005).
77. Chester, R. & Hughes, M. J. A chemical technique for the separation of ferromanganese minerals, carbonate minerals and adsorbed trace elements from pelagic sediments. *Chem. Geol.* **2**, 249–262 (1967).
78. Yang, C. et al. Geochemical perspective on large dams changing the downstream sediment sources. *J. Geochemical Explor.* **240**, 107050 (2022).
79. Copard, K. et al. Nd isotopes in deep-sea corals in the North-eastern Atlantic. *Quat. Sci. Rev.* **29**, 2499–2508 (2010).
80. Retzmann, A., Zimmermann, T., Pröfrock, D., Prohaska, T. & Irrgeher, J. A fully automated simultaneous single-stage separation of Sr, Pb, and Nd using DGA Resin for the isotopic analysis of marine sediments. *Anal. Bioanal. Chem.* **409**, 5463–5480 (2017).
81. Wombacher, F. & Rchkämpfer, M. Investigation of the mass discrimination of multiple collector ICP-MS using neodymium isotopes and the generalised power law. *J. Anal. At. Spectrom.* **18**, 1371–1375 (2003).
82. Tanaka, T. et al. JNd-1: A neodymium isotopic reference in consistency with LaJolla neodymium. *Chem. Geol.* **168**, 279–281 (2000).
83. Bouvier, A., Vervoort, J. D. & Patchett, P. J. The Lu-Hf and Sm-Nd isotopic composition of CHUR: Constraints from unequilibrated chondrites and implications for the bulk composition of terrestrial planets. *Earth Planet. Sci. Lett.* **273**, 48–57 (2008).
84. Kylander-Clark, A. R. C. et al. Coupled Lu-Hf and Sm-Nd geochronology constrains prograde and exhumation histories of high- and ultrahigh-pressure eclogites from western Norway. *Chem. Geol.* **242**, 137–154 (2007).
85. Lapen, T. J., Medaris, L. G., Beard, B. L. & Johnson, C. M. Lithos The Sandvik peridotite, Gurskøy, Norway: Three billion years of mantle evolution in the Baltica lithosphere. *LITHOS* **109**, 145–154 (2009).
86. Singer, B. S., Jicha, B. R., Fournelle, J. H., Beard, B. L. & Johnson, C. M. Lying in wait: deep and shallow evolution of dacite beneath Volcán de Santa María, Guatemala. *Geol. Soc. London, Spec. Publ.* **385**, 209–234 (2013).
87. Toucanne, S. et al. A 130,000-year record of Levantine Intermediate Water flow variability in the Corsica Trough, western Mediterranean Sea. *Quat. Sci. Rev.* **33**, 55–73 (2012).
88. Kotthoff, U. et al. Climate dynamics in the borderlands of the Aegean Sea during formation of sapropel S1 deduced from a marine pollen record. *Quat. Sci. Rev.* **27**, 832–845 (2008).

Acknowledgements

This work was funded by the projects TIMED (683237) of the European Research Council (Consolidator Grants); TRANSMOW (PID2019-105523RB-I00) from the Spanish “Agencia Estatal de Investigación” and NextData PNR 2011–2013 (<http://www.nextdataproject.it/>). The GRC Geociencias Marines thanks the Generalitat de Catalunya for the Grups de Recerca Consolidats grant 2021 SGR 01195 and for the ICREA-Academia award to I. Cacho. We thank the Universitat de Barcelona (Facultat de Ciències de la Terra, Departament de Dinàmica de la Terra i de l’Oceà) and the Università degli studi di Palermo (Scienze della Terra e del Mare) which supported the research. We also thank ISMAR-CNR (Napoli) for core NDT-6-2016 which it was recovered during the NEXTDATA expedition on board R/V CNR-Urania in 2014. We acknowledge Montse Guart, Sara Campderròs, Dimitrios Evangelinos and Judit Torner (Dept. Dinàmica de la Terra i de l’Oceà, Universitat de Barcelona) for their support with the laboratory work. Finally, we thank the editor and the anonymous reviewers for their comments, which substantially improved this manuscript.

Author contributions

S.T.-N. wrote the manuscript with support from I.C., L.P., and M.de laF.; ST-N performed the neodymium analyses with support from E.P., E.G.-S., and A.Català. N.H. performed the radiocarbon analyses. I.C. supervised the project. L.D.P., M.de laF., E.P., E.G.-S., J.F., A.Català, A.Caruso, F.L., N.H., J.N.P.-A., and I.C. discussed the results and contributed to the final manuscript.

Competing interests

The authors declare no competing interests.

Additional information

Supplementary information The online version contains supplementary material available at <https://doi.org/10.1038/s43247-023-00812-7>.

Correspondence and requests for materials should be addressed to Sergio Trias-Navarro.

Peer review information *Communications Earth & Environment* thanks the anonymous reviewers for their contribution to the peer review of this work. Primary Handling Editors: Yama Dixit and Joe Aslin. Peer reviewer reports are available.

Reprints and permission information is available at <http://www.nature.com/reprints>

Publisher’s note Springer Nature remains neutral with regard to jurisdictional claims in published maps and institutional affiliations.



Open Access This article is licensed under a Creative Commons Attribution 4.0 International License, which permits use, sharing, adaptation, distribution and reproduction in any medium or format, as long as you give appropriate credit to the original author(s) and the source, provide a link to the Creative Commons license, and indicate if changes were made. The images or other third party material in this article are included in the article’s Creative Commons license, unless indicated otherwise in a credit line to the material. If material is not included in the article’s Creative Commons license and your intended use is not permitted by statutory regulation or exceeds the permitted use, you will need to obtain permission directly from the copyright holder. To view a copy of this license, visit <http://creativecommons.org/licenses/by/4.0/>.

© The Author(s) 2023, corrected publication 2023